

# 3D fold growth rates

Marcel Frehner

Geological Institute, ETH Zurich, Sonneggstrasse 5, Zurich 8092, Switzerland

## ABSTRACT

Geological folds are inherently 3D structures; therefore, they also grow in three dimensions. Here, fold growth in all three dimensions is quantified by numerically simulating upright single-layer folds in 3D Newtonian media. Horizontal uniaxial shortening leads to a buckling instability, which grows from a point-like initial perturbation in all three dimensions by fold amplification (vertical), fold elongation (parallel to fold axis) and sequential fold growth (parallel to shortening direction) of secondary (and further) folds adjacent to the initial isolated fold. The two lateral directions exhibit similar averaged

growth rates, leading to bulk fold structures with aspect ratios in map view close to 1. However, fold elongation is continuous with increasing bulk shortening, while sequential fold growth exhibits jumps whenever a new sequential fold appears and the bulk fold structure therefore suddenly occupies more space. Compared with the two lateral growth directions, fold amplification exhibits a slightly higher growth rate.

Terra Nova, 26, 417–424, 2014

## Introduction

Geological folds are important features for structural geologists. In the field, the orientation and geometry of small-scale folds help identify larger scale structures not visible in a single outcrop (Price and Cosgrove, 1990; Ramsay and Huber, 2002). Fold structures also provide an essential basis for tectonic interpretations, for example, for estimating tectonic shortening directions. Equally important, wavelength, arclength and overall geometry of a fold are functions of the rheological parameters of the folded layer and its surrounding matrix. Therefore, analysing the fold shape can reveal information about the rheological properties of the involved rocks (Adamuszek *et al.*, 2011; Yamato *et al.*, 2011; Frehner *et al.*, 2012). Recently, Hudleston and Treagus (2010) reviewed the state-of-the-art for gaining information from fold shapes.

The fold shape observed in the field is a result of the fold growth history. Therefore, it is essential not only to describe the fold shape but also to understand the process of fold growth. Geological folds are inherently 3D structures; hence, their growth also needs to be studied in 3D.

Correspondence: Marcel Frehner, Geological Institute / NO E3, ETH Zurich, Sonneggstrasse 5, Zurich 8092, Switzerland. Tel.: +41 44 632 5468; fax: +41 44 632 1030; e-mail: marcel.frehner@erdw.ethz.ch

## Definitions of 3D fold growth

There can be confusion about the terminology of 3D fold growth. This is primarily true for the two lateral growth directions, for which various terms have been used. Fold growth parallel to the fold axis has been termed *lateral fold growth* (Bretis *et al.*, 2011; Grasemann and Schmalholz, 2012), *lateral extension* (Reber and Schmalholz, 2010) or *lateral fold propagation* (Ramsey *et al.*, 2008); for fold growth parallel to the shortening direction, the terms *lateral fold propagation* (Cobbold, 1975; Mancktelow, 1999; Schmalholz, 2008; Adamuszek *et al.*, 2013), *serial folding or buckling* (Cobbold, 1977; Schmalholz and Schmid, 2012) or *cellular buckling* (Schmalholz and Schmid, 2012) have been used. Here, *lateral fold growth* is used as an umbrella term for both lateral directions. Using *propagation* in connection with buckle folding is misleading because the governing equations describing buckling (i.e., slow viscous deformation) do not account for any propagation phenomena.

Using the coordinate system defined in Fig. 1, the following terminology for the three growth directions is used here:

- 1 *Fold amplification* ( $z$ -direction) describes the growth from a fold shape with low limb-dip angle to a shape with larger limb-dip angle.
- 2 *Fold elongation* ( $y$ -direction) is parallel to the fold axis and describes the growth from a dome-shaped (3D) structure to a more cylindrical fold (2D).

- 3 *Sequential fold growth* ( $x$ -direction) is parallel to the shortening direction and describes the growth of additional folds adjacent to the initial isolated fold. The initial fold is termed the 0th sequential fold; later grown folds are numbered consecutively.

## Fold growth in single directions

The three directions of fold growth have been studied individually in quite some detail, with fold amplification probably being the best studied direction. Various theoretical formulations exist in both 2D (Biot, 1961; Ramberg, 1963; Fletcher, 1974; Schmalholz and Podladchikov, 2000; Adamuszek *et al.*, 2013) and 3D (Ghosh, 1970; Fletcher, 1991, 1995; Mühlhaus *et al.*, 1998). Fold elongation has mainly been studied using geomorphological criteria. For example, for the Californian Wheeler and Mission Ridge anticlines (Keller *et al.*, 1999), as well as for folds in the Iranian (Ramsey *et al.*, 2008) and Iraqi Zagros Mountains (Bretis *et al.*, 2011), elongation was identified based on the drainage pattern of rivers flowing down from the growing anticlines and the distribution of wind and water gaps. Sequential fold growth from an isolated perturbation has mainly been studied in analogue (Cobbold, 1975; Abbassi and Mancktelow, 1992) and 2D numerical models (Cobbold, 1977; Lewis and Williams, 1978; Zhang *et al.*, 1996), which have also been extended to

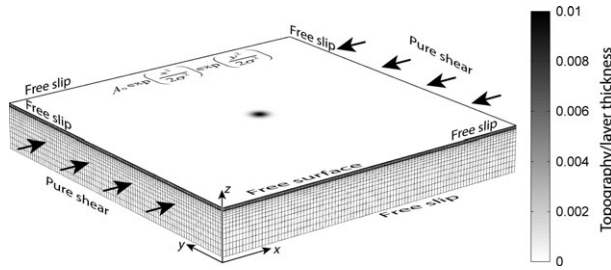


**Fig. 1** Initial numerical model grid, boundary conditions and coordinate system for studying 3D fold growth. The model consists of a higher-viscosity layer (thin layer on top) resting on a lower-viscosity layer. Grey values on the top interface represent the initial topography [Eq. (1) also given in the figure], normalized by the thickness of the top layer. Arrows indicate the pure-shear shortening boundary condition in the  $x$ -direction.

multilayer systems (Watkinson, 1976; Schmalholz and Schmid, 2012). In the Pyrenees, Espina *et al.* (1996) demonstrated sequential growth of folds based on the description of progressive unconformities.

None of the above studies considered and quantified all three growth directions at once, because they were inherently 2D studies, or because they did not focus on quantifying fold growth, or did not use a geometry or initial perturbation allowing for fold growth quantification. Analytical solutions for 3D folding (e.g., Fletcher, 1991) consider only the vertical growth of 2D initial perturbations, which are periodic (i.e., single wavelength) in the two lateral directions. The few numerical 3D folding studies (e.g., Kaus and Schmalholz, 2006; Schmid *et al.*, 2008) also do not quantify fold growth in all three directions. The aim of this study is to numerically simulate simplified test cases of 3D folding and to quantify fold growth in all three dimensions to better understand the first-order relationship between the different growth directions of a single Newtonian layer in a Newtonian media.

**Model and methods**

Buckle folding is assumed to be a slow Newtonian (linear viscous) flow process. The finite-element (FE) code that solves the corresponding continuum mechanics equations is a 3D extension of the 2D code explained in detail and benchmarked in Frehner and Schmalholz (2006), Frehner (2011), and Frehner and Exner (2014); the code can be

compared with the 3D FE code used in Schmalholz (2008) and Reber and Schmalholz (2010) and is explained in Data S1. The model (Fig. 1) consists of a higher-viscosity layer (thickness  $H_L$ ) on top of a lower-viscosity layer (thickness  $H_M$ ) with viscosity ratio  $R$ . The model has a free surface and is compressed horizontally in the  $x$ -direction with a constant background shortening strain rate,  $\dot{\epsilon}_{xx} < 0$ . This corresponds, for example, to pure-shear analogue models with lubricated base and side walls or to fold belts, where fold-axes-parallel flow is prohibited. The

initial thickness of the top layer is used as a characteristic length scale for normalizing all other lengths of the model; hence  $H_L = 1$ . The thickness of the lower viscosity layer,  $H_M$  (distance to the bottom boundary) is chosen to be large enough that matrix-controlled folding dominates ( $\frac{H_M}{H_L} \gg \frac{4}{3} (\frac{2}{3} R)^{1/3}$ ; Schmalholz *et al.*, 2002) and the exact value of  $H_M$  does not influence the results. To allow a mechanical folding instability to develop, a point-like initial perturbation is added to the bottom and top interfaces of the upper layer (Fig. 1) corresponding to a two-dimensional Gaussian,

$$G = A_0 \exp\left[\frac{x^2}{2\sigma^2}\right] \exp\left[\frac{y^2}{2\sigma^2}\right], \quad (1)$$

where  $A_0 = 0.01$ . The parameter  $\sigma$  determines the width of the initial circular perturbation in the  $x$ - and  $y$ -directions. Such an initial perturbation is different from other 3D folding studies using a random perturbation (Kaus and Schmalholz, 2006; Schmid *et al.*, 2008), but is essential here because it allows the fold structure to develop and grow from a single initiation point and hence allows fold growth to be quantified from this point. Figure 2 shows that some effective initial

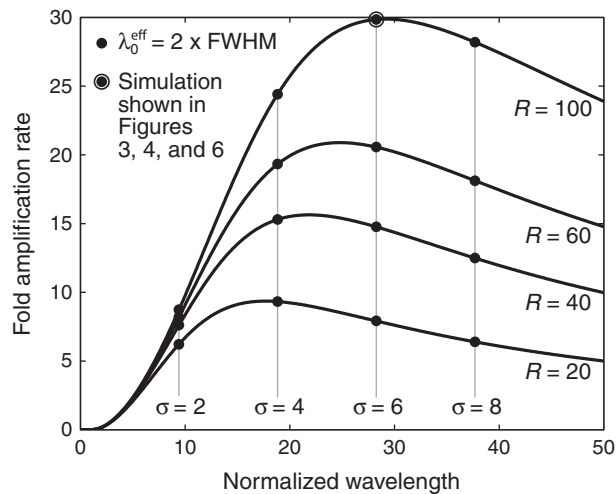


**Fig. 2** Analytically calculated fold amplification-rate spectra (z-direction) for different viscosity ratios,  $R$ , between the upper higher-viscosity layer and the underlying lower-viscosity layer according to Fletcher (1991). Dots indicate amplification-rate values for the specific values of  $\sigma$  (width of 2D Gaussian initial topography) used in the numerical simulations. The effective wavelength of the initial topography is defined as  $\lambda_0^{\text{eff}} = 2 \times \text{FWHM} = 2 \times \sqrt{8 \ln(2)} \sigma$ , where FWHM is the full width at half maximum. All lengths (wavelength, FWHM,  $\sigma$ ) are normalized by the thickness of the upper layer.

wavelengths used in the FE-simulations are shorter and some are longer than the theoretically predicted dominant wavelength.

During the FE-simulations, the bulk amplitudes (or extent) of the fold structure in all three coordinate directions are calculated based on the folded upper surface of the model:

Amplitude in  $z$ -direction:

$$A_z = z|_{x=0,y=0} - z_{\text{ref}} \quad (2)$$

Amplitude in  $y$ -direction:

$$A_y = \max(y) \text{ where } z|_{x=0} - z_{\text{ref}} = \frac{A_0}{2} \quad (3)$$

Amplitude in  $x$ -direction:

$$A_x = \max(x) \text{ where } z|_{y=0} - z_{\text{ref}} = \frac{A_0}{2} \quad (4)$$

The reference topography,  $z_{\text{ref}}$ , is the average topography of the upper model surface. Growth rates are calculated assuming exponential growth of the fold structure in all three directions as ( $t$  is time):

$$q_i = -\frac{1}{\dot{\epsilon}_{xx}t} \ln \left[ \frac{A_i}{A_i|_{t=0}} \right] + \begin{cases} -1 & \text{for } i = z \\ 0 & \text{for } i = y \\ 1 & \text{for } i = x \end{cases} \quad (5)$$

The different summands originate from the background deformation field, which kinematically amplifies the initial perturbation differently in the different directions even without an active mechanical instability. In the  $x$ -direction, the fold structure grows in the opposite direction to the background shortening; in the  $z$ -direction, the structure grows in the same direction as the kinematic background deformation; in the  $y$ -direction, there is no background extension or shortening.

Equations (2)–(5) are valid for the bulk fold structure. Similarly, amplitudes and growth rates can be calculated for each individual sequential syn- and antiform. The amplitudes in the  $z$ - and  $y$ -directions of the central fold (initial or 0th sequential fold) are equal to the bulk amplitudes.

### Results and interpretations

As a representative example, the simulation with viscosity ratio  $R = 100$

and initial perturbation  $\sigma = 6$  [Eq. (1)] is discussed below in detail and shown in Figs 3, 4 and 6. All additional simulation results for  $R = 20, 40, 60, 100$  and  $\sigma = 2, 4, 6, 8$  are summarized in Figs 5 and 7.

### Fold shape evolution and individual folds

Figure 3 shows snapshots of the evolving fold structure with increasing background shortening ( $s = 1 - \exp(-\dot{\epsilon}_{xx}t)$ ), always chosen

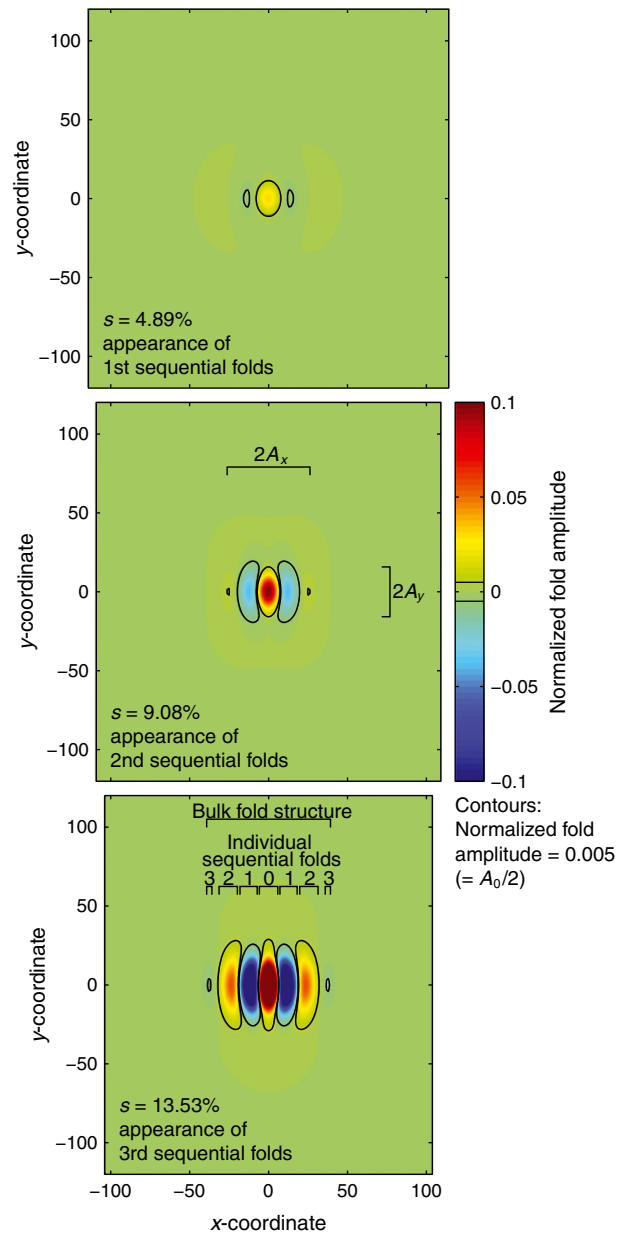


**Fig. 3** Snapshots of a typical FE-simulation showing the evolution in top-view of the 3D fold structure after different amounts of background shortening,  $s$ . Colours represent the fold amplitude ( $z$ -direction) normalized by the thickness of the top layer; black lines are contour lines of the normalized fold amplitude equal to half the initial value (0.005). Additionally, the second snapshot illustrates how the fold amplitudes in the  $x$ - and  $y$ -directions of the bulk fold structure are defined [Eqs (4) and (3)]; the third snapshot illustrates the difference between the bulk fold structure and the individual sequential folds (individual syn- and antiforms) and their numbering. Parameters for this simulation are:  $R = 100$  and  $\sigma = 6$ . A movie version of this figure, but in 3D oblique view, is available in Video S1.

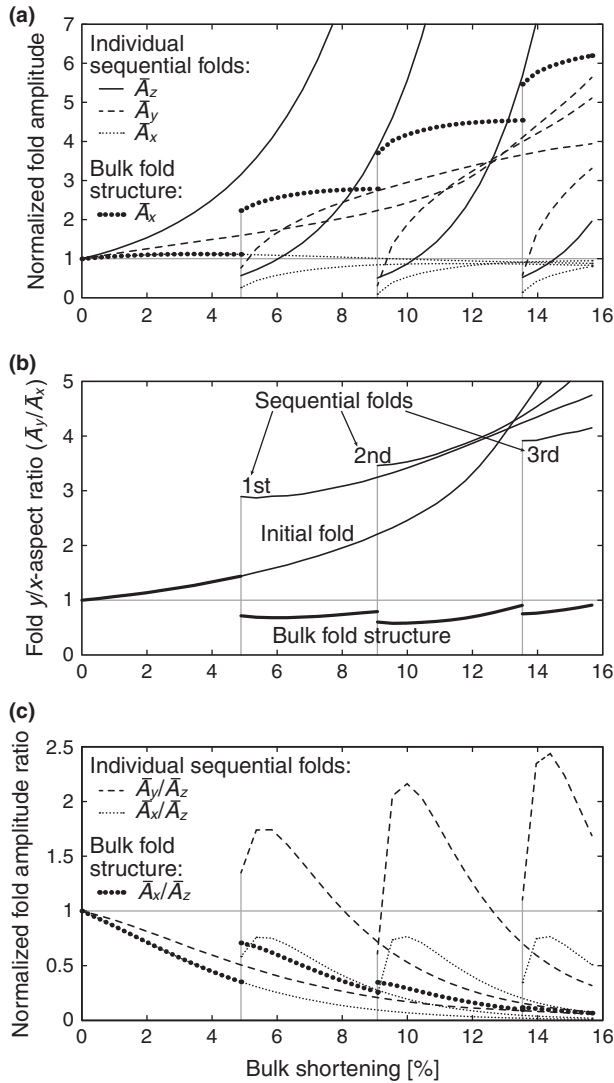


**Fig. 4** Fold amplitude evolution in all three directions (a), fold y/x-aspect ratio (b), and fold amplitude ratio (c) for both the individual sequential folds (individual anti- and synforms; thin lines) and the bulk fold structure (thick lines) with increasing bulk shortening for the same simulation as shown in Fig. 3. In the z- and y-directions, the bulk fold amplitudes are equal to the individual fold amplitudes of the initial isolated fold. All values are normalized by the initial amplitude in each corresponding direction ( $\bar{A}_x = A_x/A_{x,0}$ ,  $\bar{A}_y = A_y/A_{y,0}$ ,  $\bar{A}_z = A_z/A_{z,0}$ ). (b and c) are derived from the data shown in (a). Vertical grey lines indicate the first appearances of sequential folds.

immediately after the first appearance of new sequential  $A_0/2$  topographic contour lines. The fold shape evolution reveals growth in all three dimensions. Fold amplification (z-direction) is evident from the increasing topography (indicated by colours). Fold elongation (y-direction) is evident from the elongation of the  $A_0/2$  topographic contour line in the model centre. Sequential fold

growth (x-direction) is evident from the sequential appearance of new  $A_0/2$  topographic contour lines.

The initial isolated fold starts with normalized amplitudes (normalized by their initial values), y/x-aspect ratio (in map view), and amplitude ratios all equal to 1 (Fig. 4) representing the initial condition [Eq. (1)]. Both the z- and y-amplitudes of the individual folds increase with increas-

ing shortening. At the same time, growth in the x-direction of the individual folds is limited to an x-amplitude of around 1 (Fig. 4a) showing that the bulk fold structure grows in the x-direction by sequential folding (i.e., appearance of new individual folds) and not by the growth of one individual anti- or synform. The combination of the two lateral growths leads to an increasing y/x-aspect ratio of the initial isolated fold (Fig. 4b). New sequential folds appear with already elevated y/x-aspect ratios and continue elongating with further shortening (see also Fig. 3). Generally, fold amplitude ratios with the z-amplitude as the denominator (Fig. 4c) decrease with increasing shortening, indicating that fold growth in the z-direction exhibits a higher rate than those in the two lateral directions.

**Bulk fold amplitudes and growth rates in 3D**

Figure 4 also shows the data for the bulk fold structure (bold lines). The bulk amplitudes in the z- and y-directions are equal to those of the initial isolated fold and increase continuously with increasing shortening. Growth of the fold structure in the x-direction (Fig. 4a) is marked by sudden jumps every time a new sequential fold appears. Despite these jumps, the average amplitude in the x-direction is of the same order as that in the y-direction leading to an almost constant bulk-fold y/x-aspect ratio of around 1 (Fig. 4b). Such equal growth in both lateral directions also occurs when using different parameter combinations (Fig. 5) and seems to be a universal feature of 3D fold growth. However, these two lateral directions exhibit lower growth rates than the fold amplification (growth in the z-direction), leading to fold amplitude ratios clearly below 1 (Fig. 4c). This is also the case for other tested parameter combinations (Fig. 5). A few exceptions occur for a very short initial wavelength ( $\sigma = 2$ ), for which the very low amplification rate (Fig. 2) allows the fold structure to grow at a higher rate in the two lateral directions.

Applying Eq. (5) to the amplitude data in Fig. 4a allows the fold growth rates in all three directions to

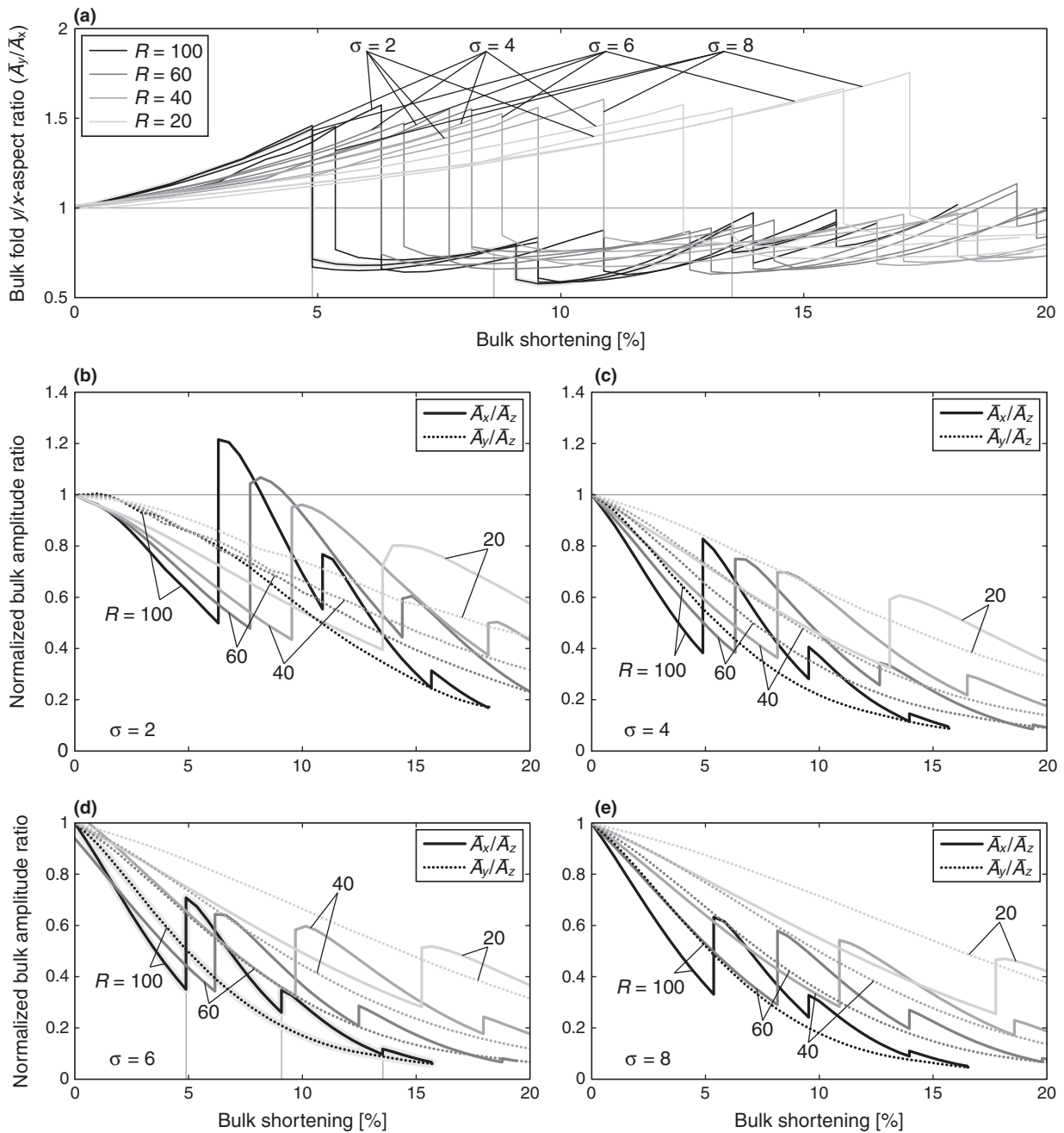


**Fig. 5** Fold  $y/x$ -aspect ratio (a) and fold amplitude ratios with the  $z$ -amplitude as the denominator (b–e) as functions of increasing shortening for different combinations of initial perturbation ( $\sigma$ -value) and viscosity ratio,  $R$ . Shown here are only the curves for the bulk fold structure. The line grey scale corresponds to different viscosity ratios,  $R$ , between the upper higher-viscosity layer and the underlying lower-viscosity layer. The fold  $y/x$ -aspect ratio of all simulations is shown in a single sub-figure (a), while for readability reasons the fold amplitude ratio is distributed across four sub-figures (b–e). The curves shown in Fig. 4b and c ( $R = 100, \sigma = 6$ ) are decorated with a light grey background. All values are normalized by the initial amplitude in each corresponding direction ( $\bar{A}_x = A_x/A_{x,0}, \bar{A}_y = A_y/A_{y,0}, \bar{A}_z = A_z/A_{z,0}$ ).

be calculated (Fig. 6). The initial fold amplification rate ( $z$ -direction) of around 19 is smaller than the value theoretically predicted for this simu-

lation (Fig. 2; Fletcher, 1991). This initial discrepancy arises because the theoretical prediction is valid only for a periodic initial perturbation

(single wavelength), while the Gaussian perturbation used in the FE-simulation contains the entire wavelength spectrum and therefore

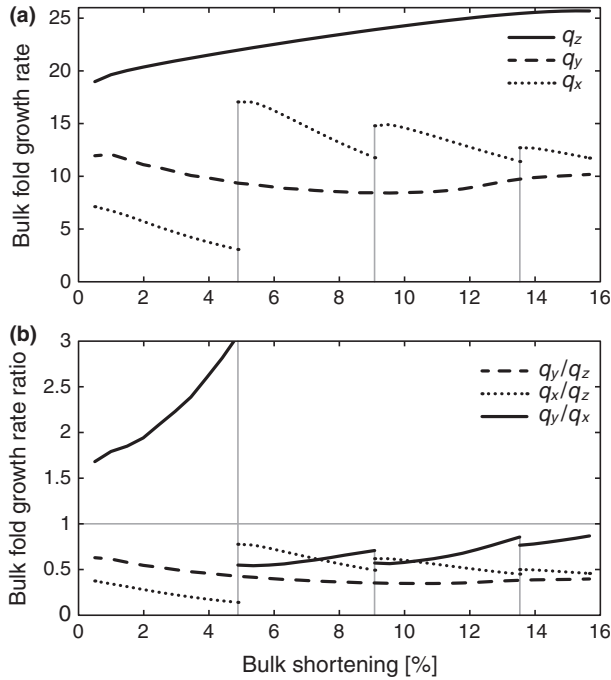


**Fig. 6** Fold growth rates in all three directions (a) and the ratios between fold growth rates (b) for the bulk fold structure with increasing shortening for the same simulation as shown in Figs 3 and 4. (a) is derived by applying Eq. (5) to the data shown in Fig. 4a. (b) is derived from the data shown in (a). Vertical grey lines indicate the first appearance of sequential folds.

also wavelengths that grow at a smaller rate. The fold amplification rate increases slightly with increasing shortening (Fig. 6a), while the fold elongation rate ( $y$ -direction) stays roughly constant at a value of around 10. The sequential fold growth rate ( $x$ -direction) exhibits jumps when new sequential folds appear. In the long term, both lateral fold-growth rates are similar, represented by a lateral growth rate ratio close to 1 (Fig. 6b), and about half the fold amplification rate (growth rate ratio around 0.5). This general relationship between the different fold growth rates is confirmed by all other parameter combinations (Fig. 7).

**Discussion and conclusions**

Even though fold growth in all three directions is the result of the same mechanical buckling instability, the mode of growth in the three directions is different. Fold amplification and elongation are primarily related to the growth of the initial isolated fold, while

sequential fold growth is due to the consecutive appearance of new folds. Additionally, growth in the two lateral directions results in the involvement of more and more rock material further away from the initial perturbation, while fold amplification does not incorporate significantly more material with increasing shortening.

The numerical simulations represent simplified test cases. They only comprise a two-layer system, linear viscous (Newtonian) rheology, a single initial perturbation, no erosion at the upper surface and no gravity. Erosion (Simpson, 2004) and gravity (Schmalholz *et al.*, 2002) can increase and reduce the fold amplification rate, respectively; yet their influence on the two lateral growth rates remains to be studied. The aim of this study was to demonstrate first-order phenomena of 3D fold growth of a single structure, and the modelled geometries may not be translated one-to-one to natural fold structures. In nature, or in models using random

initial perturbation, several individual fold structures may initiate synchronously from a multitude of perturbations and later link with each other. The presented results illustrate that sequential fold growth may be as important as fold elongation for understanding the linkage between initially isolated fold structures resulting in linked structures with large  $y/x$ -aspect ratio (Grasemann and Schmalholz, 2012).

The lack of erosion and gravity prevents the simulation results from being directly compared with large-scale near-surface folds, such as in the Zagros Mountains. However, the general result of almost equal fold growth rates in both lateral directions and a slightly larger fold growth rate in the vertical direction is expected to hold in more realistic modelling scenarios or natural situations. If a fold structure originates from an isolated circular initial perturbation (e.g., a diapir), its bulk  $y/x$ -aspect ratio remains roughly 1 : 1. Even though the final fold geometry in an appropriate  $y$ - $z$ -cross-section may be 2D, the evolution leading to this geometry is fully 3D and a mechanical 2D description may be inappropriate. If a fold structure originates from a line perturbation (e.g., a basement fault), its bulk  $y/x$ -aspect ratio remains large. In this case, approximating the fold as a 2D structure, both geometrically and mechanically, is valid.

The presented simulations cover the early stages of folding (<20% shortening). Various studies (e.g., Schmalholz and Podladchikov, 2000; Schmalholz, 2006; Adamuszek *et al.*, 2013) have demonstrated that the amplification rate decreases at later folding stages. Whether the two lateral fold growth rates also decrease or whether the lateral growths outpace the vertical growth remains to be studied. However, such numerical simulations may be challenging because they require a very large domain in the  $x$ - $y$ -direction to capture the two lateral growths without boundary effects. Future work may focus on the effect of different tectonic regimes (i.e., boundary conditions) such as transpression and transtension.

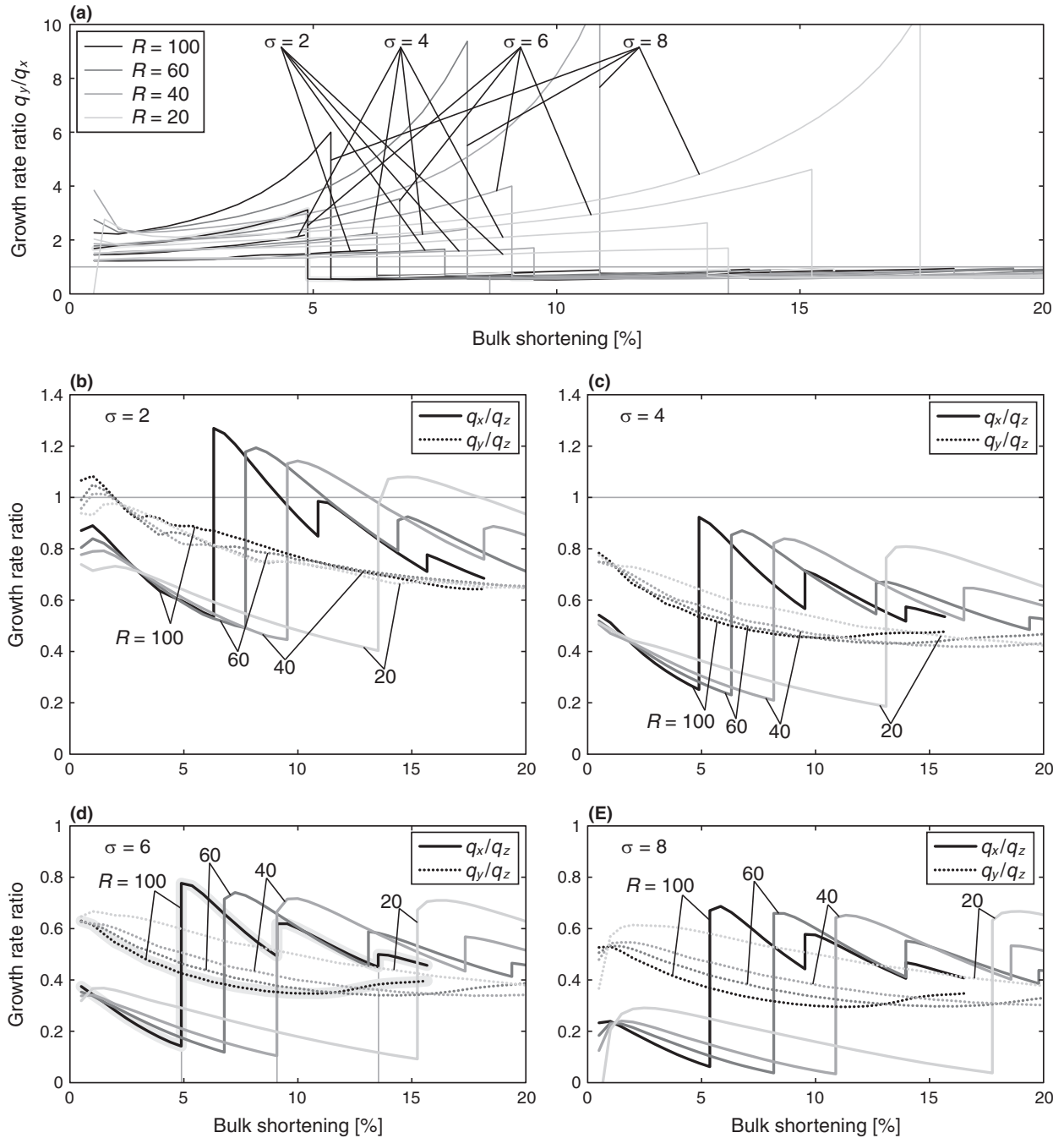


**Fig. 7** Ratio between the two lateral fold growth rates (a) and ratios between fold growth rates with the  $z$ -growth rate as the denominator (b–e) as functions of increasing shortening for different combinations of initial perturbation ( $\sigma$ -value) and viscosity ratio,  $R$ . Shown here are only the curves for the bulk fold structure. The line grey scale corresponds to different viscosity ratios,  $R$ , between the upper higher-viscosity layer and the underlying lower-viscosity layer. The ratio between the two lateral fold growth rates of all simulations is shown in a single sub-figure (a), while for readability reasons, the ratios between fold growth rates with the  $z$ -growth rate as the denominator are distributed across four sub-figures (b–e). The curves shown in Fig. 6 ( $R = 100, \sigma = 6$ ) are decorated with a light grey background.

## Acknowledgements

Discussion with and feedback from Neil Mancktelow and Naiara Fernandez are greatly acknowledged. This work was supported by the ETH Zurich, Switzerland.

## References

- Abbassi, M.R. and Mancktelow, N.S., 1992. Single layer buckle folding in nonlinear materials – I. Experimental study of fold development from an isolated initial perturbation. *J. Struct. Geol.*, **14**, 85–104.
- Adamuszek, M., Schmid, D.W. and Dabrowski, M., 2011. Fold geometry toolbox – Automated determination of fold shape, shortening, and material properties. *J. Struct. Geol.*, **33**, 1406–1416.
- Adamuszek, M., Schmid, D.W. and Dabrowski, M., 2013. Theoretical analysis of large amplitude folding of a single viscous layer. *J. Struct. Geol.*, **48**, 137–152.
- Biot, M.A., 1961. Theory of folding of stratified viscoelastic media and its implications in tectonics and orogenesis. *Geol. Soc. Am. Bull.*, **72**, 1595–1620.
- Bretis, B., Bartl, N. and Grasemann, B., 2011. Lateral fold growth and linkage in the Zagros fold and thrust belt (Kurdistan, NE Iraq). *Basin Res.*, **23**, 615–630.
- Cobbold, P.R., 1975. Fold propagation in single embedded layers. *Tectonophysics*, **27**, 333–351.
- Cobbold, P.R., 1977. Finite-element analysis of fold propagation – A problematic application? *Tectonophysics*, **38**, 339–353.
- Espina, R.G., Alonso, J.L. and Pulgar, J.A., 1996. Growth and propagation of buckle folds determined from syntectonic sediments (the Ubierna Fold Belt, Cantabrian Mountains, N Spain). *J. Struct. Geol.*, **18**, 431–441.
- Fletcher, R.C., 1974. Wavelength selection in folding of a single layer with power-law rheology. *Am. J. Sci.*, **274**, 1029–1043.
- Fletcher, R.C., 1991. Three-dimensional folding of an embedded viscous layer in pure shear. *J. Struct. Geol.*, **13**, 87–96.
- Fletcher, R.C., 1995. Three-dimensional folding and necking of a power-law layer: are folds cylindrical, and, if so, do we understand why? *Tectonophysics*, **247**, 65–83.
- Frehner, M., 2011. The neutral lines in buckle folds. *J. Struct. Geol.*, **33**, 1501–1508.
- Frehner, M. and Exner, U., 2014. Strain and foliation refraction patterns around buckle folds. In: *Deformation Structures and Processes within the Continental Crust* (S. Llana-Fúnez, A. Marcos and F. Bastida, eds). *Geol. Soc. London Spec. Publ.*, **394**, 21–37.
- Frehner, M. and Schmalholz, S.M., 2006. Numerical simulations of parasitic folding in multilayers. *J. Struct. Geol.*, **28**, 1647–1657.
- Frehner, M., Reif, D. and Grasemann, B., 2012. Mechanical versus kinematical shortening reconstructions of the Zagros High Folded Zone (Kurdistan Region of Iraq). *Tectonics*, **31**, TC3002.
- Ghosh, S.K., 1970. A theoretical study of intersecting fold patterns. *Tectonophysics*, **9**, 559–569.
- Grasemann, B. and Schmalholz, S.M., 2012. Lateral fold growth and fold linkage. *Geology*, **40**, 1039–1042.
- Hudleston, P.J. and Treagus, S.H., 2010. Information from folds: a review. *J. Struct. Geol.*, **32**, 2042–2071.
- Kaus, B.J.P. and Schmalholz, S.M., 2006. 3D finite amplitude folding: implications for stress evolution during crustal and lithospheric deformation. *Geophys. Res. Lett.*, **33**, L14309.
- Keller, E.A., Gurrrola, L. and Tierney, T.E., 1999. Geomorphic criteria to determine direction of lateral propagation of reverse faulting and folding. *Geology*, **27**, 515–518.
- Lewis, R.W. and Williams, J.R., 1978. A finite-element study of fold propagation in a viscous layer. *Tectonophysics*, **44**, 263–283.
- Mancktelow, N.S., 1999. Finite-element modelling of single-layer folding in elasto-viscous materials: the effect of initial perturbation geometry. *J. Struct. Geol.*, **21**, 161–177.
- Mühlhaus, H.-B., Sakaguchi, H. and Hobbs, B., 1998. Evolution of three-dimensional folds for a non-Newtonian plate in a viscous medium. *Proc. Roy. Soc. London A Math. Phys. Eng. Sci.*, **454**, 3121–3143.
- Price, N.J. and Cosgrove, J.W., 1990. *Analysis of Geological Structures*. Cambridge University Press, Cambridge. ISBN 0-521-31958-7.
- Ramberg, H., 1963. Fluid dynamics of viscous buckling applicable to folding of layered rocks. *AAPG Bulletin*, **47**, 484–505.
- Ramsay, J.G. and Huber, M.I., 2002. *The Techniques of Modern Structural Geology, Volume 2: Folds and Fractures*. Academic Press, London. ISBN 0-12-576922-9.
- Ramsey, L.A., Walker, R.T. and Jackson, J., 2008. Fold evolution and drainage development in the Zagros mountains of Fars province, SE Iran. *Basin Res.*, **20**, 23–48.
- Reber, J.E. and Schmalholz, S.M., 2010. Stress orientation and fracturing during three-dimensional buckling: numerical simulation and application to chocolate-tablet structures in folded turbidites, SW Portugal. *Tectonophysics*, **493**, 187–195.
- Schmalholz, S.M., 2006. Scaled amplification equation: a key to the folding history of buckled viscous single-layers. *Tectonophysics*, **419**, 41–53.
- Schmalholz, S.M., 2008. 3D numerical modeling of forward folding and reverse unfolding of a viscous single-layer: implications for the formation of folds and fold patterns. *Tectonophysics*, **446**, 31–41.
- Schmalholz, S.M. and Podladchikov, Y.Y., 2000. Finite amplitude folding: transition from exponential to layer length controlled growth. *Earth Planet. Sci. Lett.*, **179**, 363–377.
- Schmalholz, S.M. and Schmid, D.W., 2012. Folding in power-law viscous multi-layers. *Philos. Trans. Roy. Soc. A Math. Phys. Eng. Sci.*, **370**, 1798–1826.
- Schmalholz, S.M., Podladchikov, Y.Y. and Burg, J.-P., 2002. Control of folding by gravity and matrix thickness: implications for large-scale folding. *J. Geophys. Res.*, **107**, ETG 1-1–ETG 1-16.
- Schmid, D.W., Dabrowski, M. and Krotkiewski, M., 2008. Evolution of large amplitude 3D fold patterns: a FEM study. *Phys. Earth Planet. Inter.*, **171**, 400–408.
- Simpson, G., 2004. Role of river incision in enhancing deformation. *Geology*, **32**, 341–344.
- Watkinson, A.J., 1976. Fold propagation and interference in a single multilayer unit. *Tectonophysics*, **34**, T37–T42.
- Yamato, P., Kaus, B.J.P., Mouthereau, F. and Castelltort, S., 2011. Dynamic constraints on the crustal-scale rheology of the Zagros fold belt, Iran. *Geology*, **39**, 815–818.
- Zhang, Y., Hobbs, B.E., Ord, A. and Mühlhaus, H.B., 1996. Computer simulation of single-layer buckling. *J. Struct. Geol.*, **18**, 643–655.

Received 12 February 2014; revised version accepted 30 June 2014

## Supporting Information

Additional Supporting Information may be found in the online version of this article:

**Data S1.** Description of finite-element code.

**Video S1.** Animated movie version of Fig. 3, but in 3D oblique view.